

Investigation of Radial Shaft Seal Swelling Using a Special Tribometer and Magnetic Resonance Imaging

Daniel Bellaire,[▽] Stefan Thielen,[▽] Christoph Burkhardt,[▽] Kerstin Münnemann,* Hans Hasse, and Bernd Sauer



Cite This: *ACS Omega* 2022, 7, 11671–11677



Read Online

ACCESS |



Metrics & More

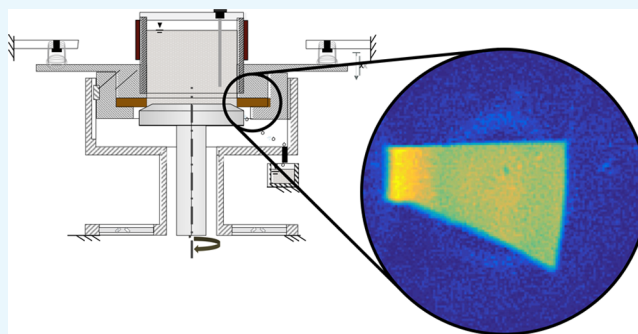


Article Recommendations



Supporting Information

ABSTRACT: Compatibility between the rubber material of radial shaft seals and the lubricants to be sealed is an important requirement that customers demand of their lubricant suppliers. Among other effects that may result from incompatibility, the penetration of lubricant components into the rubber (swelling) can impair the seal's functionality due to changes in its geometry and mechanical behavior. Typically, the penetration of a lubricant into an elastomer is evaluated after an immersion test using volumetric, gravimetric, and extraction measurements. Due to the small changes that need to be detected, such methods may not be sufficient to obtain meaningful results. In this contribution, we use magnetic resonance imaging (MRI) to investigate swelling on special tribometer samples as well as a radial shaft seal that were previously used in component tests. Several combinations of rubbers and lubricants that have proven to be compatible were tested in addition to combinations with expected incompatibilities in real applications. The results indicate that MRI measurements can be used to quantify the penetration depth and potentially also the velocity with which the lubricant diffuses into the rubber, thereby yielding detailed insights into the swelling process of the seal.



INTRODUCTION

The primary function of radial shaft seals (RSS) is to keep the lubricant inside a machine while allowing for the relative motion of a shaft at its exit from the machine.¹ During shaft rotation, the friction in the sealing contact will cause a significant overtemperature.² The tribological conditions in the contact zone accelerate interactions between the rubber material of the seal and the lubricant and may impair the functionality of the sealing system. This is designated as incompatibility between the lubricant and the rubber.^{3–7} Of all long-term seal failures, 40% can be attributed to lubricant incompatibility.⁸

The main function of the lubricants is to improve the tribological conditions in the contact between machine elements such as gears or bearings inside the machine. Therefore, a lubricant is primarily optimized with regard to its function within those contacts at the given operation conditions. However, undesired chemical and physical interactions with the material of the shaft seal must also be ruled out when pairing a lubricant and a seal material. Typically, customers prescribe compatibility with the seal as a requirement that the lubricant provider has to fulfill.

Rubber and lubricant components typically interact with each other, primarily causing changes of the rubber's properties. The underlying mechanisms can be classified into chemical and physical interactions. Physical interactions

include the extraction of rubber components (fillers and softeners) into the lubricant and the diffusion of lubricant components (base oil and additives) into the rubber. Usually, the latter effect, which usually leads to swelling and is often labeled as such, is more dominant.⁹ Chemical interactions describe changes of the seal material due to chemical reactions with lubricant components.

Current compatibility tests are based on static immersion tests, which typically use flat 2 mm thick slabs or similar simplified geometries, and also functional testing on real parts. While static immersion tests are standardized in DIN ISO 1817:2016-11¹⁰ and ISO 6072:2011,¹¹ dynamic tests using real seals are usually found in internal testing protocols of companies and therefore represent those company's specific application conditions.^{12,13} The conditions of static immersion tests differ very often considerably from the application and can lead to wrong interpretations and conclusions, since dynamic conditions often combine thermal, mechanical, and chemical loads during exposure to a certain medium. The real

Received: November 19, 2021

Accepted: March 7, 2022

Published: March 31, 2022



contact temperature with respect to sealing applications is much higher than the bulk oil temperature, which is usually used as the reference temperature in static immersion tests. It has been shown that some incompatibilities can even be provoked or accelerated in real contact conditions,⁸ which would mean that critical changes in the contact zone of the RSS could be missed in a static test. In a study by Klaiber et al.,⁵ no correlations were found between changes in rubber properties during a static test and another dynamic test with an identical RSS.

After conducting compatibility tests, incompatibility effects have to be investigated on the rubber specimen. Especially in the case of static tests, where any specimen geometry can be realized, such tests pose no challenge. Changes in mechanical properties can be determined using tensile tests, hardness measurements, or dynamic mechanical thermal analysis (DMTA). Swelling can also be easily quantified using volumetric and gravimetric investigations in static tests where no wear-related mass loss is suspected. For example, the lubricant components that have penetrated the rubber could be identified using gas chromatography–mass spectrometry (GC-MS). The investigation of changes in seals after dynamic testing is not as easy, e.g., the seal geometry may not allow for the preparation of a tensile test specimen. Therefore, functional characteristics of the seal such as wear, contact width, radial force, leakage, and friction torque are typically used to characterize the effects of incompatibility.^{13,14} X-ray photoelectron spectroscopy (XPS) studies on swollen elastomer slices give insight into the penetration depth of lubricants.¹⁵ Contrary to XPS measurements, magnetic resonance imaging (MRI) does not require a physical modification, i.e., slicing of the sample, in the region of interest.

The ring cone tribometer used in this study was developed to represent a tribologically equivalent system for a RSS. It has been optimized to be very comparable to a sealing system with a RSS in terms of friction, wear, and contact temperature.^{16,17} In a current research project, investigations on whether the tribometer can be used for dynamic incompatibility testing in very early stages of lubricant development when only a small amount of lubricant has been mixed (lab-scale) are in progress. Usually, the dynamic incompatibility tests on rubber seals are conducted at a later and therefore more costly lubricant development stage when much more lubricant is available to fulfill the needs of such conventional tests. Very early compatibility tests would therefore have the potential to prevent expensive investments in the development of incompatible lubricant test batches at a larger scale. Such dynamic compatibility tests are associated with high costs. The ring cone tribometer has the potential to reduce costs using a specimen with a simple geometry and less lubricant.

As part of this work, we investigated the possibility of using MRI to identify lubricant components that have penetrated the rubber samples. Different combinations of rubber and lubricant with known swelling problems and combinations with good compatibility have been tested on the tribometer and also in RSS tests. After the test, those samples were subjected to ex situ MRI measurements at room temperature and ambient pressure without further mechanical stress.

The development of the MRI technique was largely driven by biomedical sciences, but its application in the natural and engineering sciences soon followed.¹⁸ To obtain a magnetic resonance image, dynamic magnetic gradient fields are superimposed on the static magnetic field, which is used to

generate the NMR signal. The use of gradient fields results in the space dependency of the NMR signal, which can be converted into an image via Fourier transformation. The technique was soon adopted for the structural investigation of elastomers.^{19–23} The studied topics include the oxidative aging²⁴ and cross-link density^{25–27} of the investigated materials. Furthermore, the penetration of different solvents^{28–35} into elastomers has been investigated. All the above-mentioned studies employed (frequency-encoding) spin–echo or gradient echo techniques or variants of them. A prerequisite for the use of these techniques is a sufficiently long T_2 relaxation time. If the sample's T_2 relaxation happens too fast, i.e., is on the order of the duration of the pulse sequence, the NMR signal may be too weak to resolve or completely gone by the time of acquisition. This is illustrated well in a study by McDonald,³⁶ where only the solvent is visible penetrating into the dark (i.e., giving no signal) elastomer. This is because of the very different relaxation times of the elastomer and the solvent. The swollen elastomer, however, is also visible owing to the increase of its relaxation time due to the solvent penetration, which hampers the quantification of the solvent take-up. To check an elastomer for solvent penetration, it is advantageous to be able to record the nonswollen elastomer and the solvent simultaneously. Consequently, imaging techniques have to be employed that alleviate the problem of fast elastomer relaxation. One of those methods is single-point imaging (SPI).³⁷ SPI is purely based on phase-encoding and sampling of only a single data point per acquisition instead of a whole line of data in k -space. As a consequence, the duration for the pulse sequence is minimized and, furthermore, only the strongest part of the NMR signal, that is unattenuated due to relaxation, is recorded. As a further advantage, many of the artifacts that plague other pulse sequences are not observed when the SPI sequence is used. The main disadvantage is a prolonged measurement time compared to frequency-encoding techniques. Application of SPI for the investigation of elastomers has been shown to produce images with good resolution,^{38,39} even in three spatial dimensions.⁴⁰ In this work, spin density images of elastomer samples were recorded with the SPI method to determine any lubricant penetration after the seals were subjected to a representative tribological process. If lubricant penetration was observed, the penetration depth was determined. Furthermore, 3D imaging of an RSS of a more complex geometry is demonstrated. To the best of our knowledge, there are no reports in the literature on studies in which the results of application-like wear tests are monitored by MRI, as it is done in the present study.

This paper is organized as follows: In the section **Materials and Methods**, the sample preparation and the measurement method are detailed. This includes the description of the samples, the tribological processing, the preparation of the sample for the MRI measurement, the MRI method, and the MRI parameters used. In the section **Results**, the obtained images of the elastomer samples are presented and analyzed. The findings of the study are summarized in the **Conclusion**.

■ MATERIALS AND METHODS

The dynamic aging process was conducted on the ring cone tribometer (RFT). The scheme of the test rig is depicted in **Figure 1**. The test rig uses simple ring-shaped flat elastomer specimen (**Figure 2**) and a coned shaft. The cone angle was chosen to imitate the contact angles of the RSS. It has been

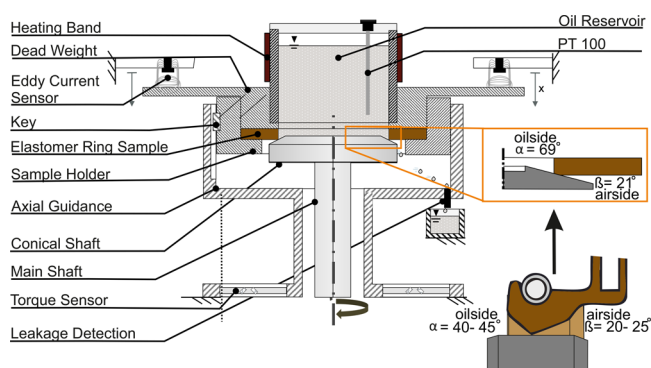


Figure 1. The ring cone tribometer (RFT). Scheme of the ring cone tribometer test rig and the analogy to RSS in terms of their contact angles.

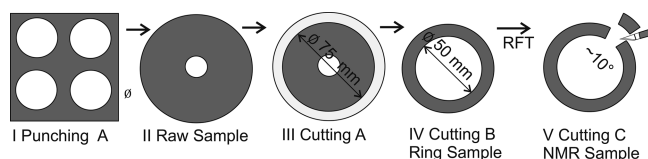


Figure 2. Ring sample production process. (I) The raw samples are punched out from a 2 mm thick flat-molded elastomer slab. (II) The raw samples are shaped with a lathe in a two-step cutting process to the original shape with (III) an outer diameter of 75 mm and (IV) an inner diameter of 50 mm. This sample size can be tested in the RFT test rig. (V) After the test, an approximately 10° wide piece was cut out for MRI analysis.

optimized based on contact simulations and experiments and can be easily configured for any specific shaft seal.¹⁶ During the test, the elastomer sample slides on the cone. The whole system is lubricated with a small amount of test oil in the reservoir above the contact zone. Only 100 mL of lubricant is necessary for a single test, which can be heated up to 150 °C. The tribometer has successfully been used to reproduce the friction and wear behavior of a common RSS.¹⁶

To achieve tribologically equivalent operation conditions, the relative sliding velocity v_s and line load p_l of the RFT should be chosen to be as close to the RSS as possible. The line load of the seal can be determined by measuring the radial force determined at the application temperature and the seal contact length.¹⁶ The application of dead weights leads to a constant line load during the test. A consideration of the cone angle is necessary when calculating the weight for the desired line pressure.

During the wear process, the whole sample holder moves downward. The axial movement of the test cell can be monitored with an online wear measurement system based on eddy current sensors.¹⁷ This is illustrated in Figure 3. While the signal for sample I shows an increase in distance due to the wear-related lowering of the sample holder, sample III shows a decrease in the distance signal, hinting at the sample holder raising due to a swelling-related expansion of the rubber sample in the contact area. Further details about the working principle and the online wear measurement can be found in previous studies.^{16,17}

To supply samples of dynamically aged and stressed elastomer materials, a series of tests was performed on the ring cone tribometer. Compatible and incompatible combinations of seals and lubricants were tested (compare Table 1). The compatibility was judged based on reports of the sealing

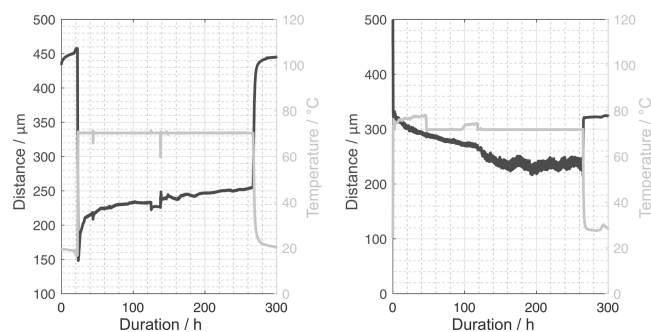


Figure 3. Online wear measurement. Axial movement of the ring sample specimen and its sample holder during a tribological test in the case of elastomer–lubricant combination I due to wear (left) and in the case of combination III due to wear combined with swelling (right).

Table 1. Elastomer–Lubricant Combinations That Were Used in This Study^a

sample no.	elastomer	lubricant	ISO VG	shaft	compatibility
I	75 FKM S85	PAO	220	AISI 5115	++
II	75 FKM S85	PAG I	68	AISI 5115	–
III	70 ACM 121433	PAG II	220	AISI 5115	– – –
IV	70 ACM 121433 ^b	MIN	220	AISI 5115	=

^aPAO = polyalphaolefin, PAG = polyalkylene glycol, MIN = mineral oil, + represents compatible, – represents incompatible, and = represents neutral. ^bRadial shaft seal.

performance during the wear process. Additionally, the expectation for the compatibility based on prior knowledge from other studies is specified (compare the Supporting Information). The test parameters and the conditions of each test are summarized in Table 2.

A highly resistant industrial fluoroelastomer (FKM) was combined with a polyalphaolefin (PAO) lubricant of the ISO VG 220 class ($\rho_{20} = 857.9 \text{ kg/m}^3$ and $\nu_{40} = 228.1 \text{ mm}^2/\text{s}$) for a baseline test (sample I). The PAO was blended with a small amount of ester to achieve better solubility of the antifoam and antioxidant additives included in this lubricant. Apart from that, no further additives, for example, those to enhance the tribological performance, were incorporated. Based on prior knowledge,⁴² when the ester content is just above 5%, a high compatibility and therefore no significant diffusion of the lubricant into the sealing lip region is assumed for this combination. The same elastomer was combined with a polyalkylene glycol (PAG) lubricant (ethylene oxide/propylene oxide random copolymer monobutyl ether) from the ISO VG 68 class ($\rho_{20} = 1036.0 \text{ kg/m}^3$ and $\nu_{40} = 70 \text{ mm}^2/\text{s}$) under similar test conditions but a higher oil sump temperature. This lubricant–elastomer combination is, due to its unpolar nature, much more prone to swelling compared to PAO lubricants (sample II). A limited compatibility was certified based on a swelling of 23% after static immersion at 100 °C for 40 days.⁴² An alkyl acrylate copolymer (ACM) was combined with a polyalkylene glycol of the ISO VG 220 class ($\rho_{20} = 1054.4 \text{ kg/m}^3$ and $\nu_{40} = 240.57 \text{ mm}^2/\text{s}$) for the third test (sample III). For both combinations (sample II and sample III), incompatibility has been reported based on observations of

Table 2. Test Parameters for the Different Elastomer–Lubricant Combinations^a

sample no.	duration	speed	distance	line load	oil temperature	leakage
I	336 h	5 m/s	6084 km	0.14 N/mm	70 °C	T
II	336 h	5 m/s	6084 km	0.12 N/mm	90 °C	L
III	278 h	5 m/s	5000 km	0.14 N/mm	70 °C	L
IV	116 h	**	5000 km	0.147 N/mm	70 °C	L

^aT indicates tight, L indicates leakage, and ** indicates the dynamic test cycle according to ref 41.

the performance in seal tests.^{42,43} The PAG incorporates antioxidants and an additive package, which is not further specified. Up to four samples were tested at the same time on the test rig. From those samples, one specimen was selected for MRI analysis.

The study was completed with an RSS component test on a multishaft test bench.⁴⁴ Seals were used according to DIN 3760 A80-100-10. The seals were molded from the same ACM material as that in sample III and combined with a mineral lubricant (MIN) with an additive package for industrial use. The composition of the additive content of this lubricant was unknown. Test parameters and the test cycle were selected according to an FVA reference.⁴¹ After a 5 h runtime at 1200 rpm, the samples were tested in a cyclic test stage with nine stages from 500 to 4500 rpm in 500 rpm steps. Every step had a duration of 120 min. After this stage, the seals were tested at a constant speed of 3200 rpm. At the end of the entire test cycle, the cyclic stages were repeated once again. Except for sample I, leakage was reported during all test cycles, leading to the assumption that, apart from sample I, the material combinations did not harmonize well.

After the tribological test, the samples were removed from the sample holder. The elastomer specimen were carefully cleaned of the test lubricant using ethanol and an ultrasonic bath for 10 min. This is necessary to remove any iron-containing particles that could be attached to the surface prior to MRI analysis. Afterward, a small section was cut from the elastomer ring samples using a sharp scalpel (compare Figure 2). This was necessary due to the restricted dimensions of the MRI coil. The same procedure was repeated for the RSS. Here, part of the sealing lip was cut off from the rest of the seal at the membrane of the RSS to provide a metal-free sample for MRI analysis. Similar to the ring samples, the sealing lip was also sectioned to provide a 10° segment.

¹H spin density images were recorded with a Bruker Biospin NMR spectrometer with a magnetic field strength of 7.05 T, corresponding to a proton Larmor frequency of 300.13 MHz (Ascend 300 wide bore magnet and an Avance Neo console). Imaging capabilities are realized by a microimaging probe (Micro 2.5, 30 mm diameter) with a ¹H quadrature detection coil. The acquisition software was Paravision 360, which was also used to render the 3D images. SPI⁴⁵ was used for the acquisition. SPI applies a $\pi/2$ pulse that generates a free induction decay (FID) signal. The FID signal is spatially encoded using phase gradients in all spatial directions. Immediately afterward at a fixed time in the pulse sequence, a single data point of the FID is recorded. The evolution time spans from the $\pi/2$ pulse to the point of acquisition and is a lot shorter than that used for typical echo-based MRI, thereby allowing the acquisition of fast-decaying signals. Another distinct advantage is the lack of time-evolution artifacts (e.g., by chemical shift or magnetic susceptibility), since the time evolution of the signal is not recorded. The drawback of the method is its long measurement time since, from every FID

signal, only a single point of *k*-space (hence the name of the sequence: single point imaging) is sampled instead of a whole line, as it is the case for frequency-encoding methods. The fully sampled *k*-space is then translated into the two-dimensional (2D) or three-dimensional (3D) image by Fourier transformation. The pixel (2D) or voxel (3D) intensities in the image are proportional to the proton concentration resulting from any elastomer material and the solvent in the measured volume. Consequently, the experimental data do not distinguish between the elastomer and the solvent. However, distinguishing between the elastomer and the solvent is possible qualitatively based on shapes in the resulting pixel (or voxel) image. By comparing regions of the solvent-free elastomer and the elastomer into which solvent has penetrated, a relative quantification of the solvent penetration is also possible.

Table 3 lists the used experimental parameters for the 2D and 3D MRI acquisitions. The spatial resolution for all images

Table 3. Pulse Sequence Parameters That Were Used in This Work

	SPI (2D)	SPI (3D)
field of view (mm)	30 × 30	20 × 20 × 10
size (pixels)	128 × 128	128 × 128 × 8
evolution time (ms)	0.072	0.072
repetition time (ms)	3	3
flip angle (°)	3	3
signal averages	2048	2048
acquisition time (h)	21	105.5

is 0.16 mm per pixel. A conical field of view was used as it still encompassed the whole sample and took significantly less measurement time than a Cartesian field of view.

RESULTS

Figure 4 shows MRI images of the samples I, II, and III. Good images for all investigated elastomer samples were obtained with the SPI method, which is not trivial.³⁶ All images show a sufficient signal-to-noise ratio (SNR), and the geometry of the elastomers can be visualized very well with a high spatial resolution of 0.16 mm. The images show only minor artifacts, i.e., in the images of sample II (bright pixel at the bottom) and sample III (round shadow near the elastomer). For a more detailed investigation of the oil penetration into the seal, intensity profiles are depicted below the MRI images in Figure 4. The profiles were obtained by averaging the intensities from ten pixel lines (indicated by the red rectangle in the MRI images) to improve the SNR. The profiles are basically taken in the radial direction in the seal, cf. Figure 4.

On first sight, the softest compound, i.e. sample III, offers the best SNR. For the other samples, the SNRs are slightly lower. For samples II and III, a higher intensity near the sealing edge is visible, which indicates the penetration of lubricant

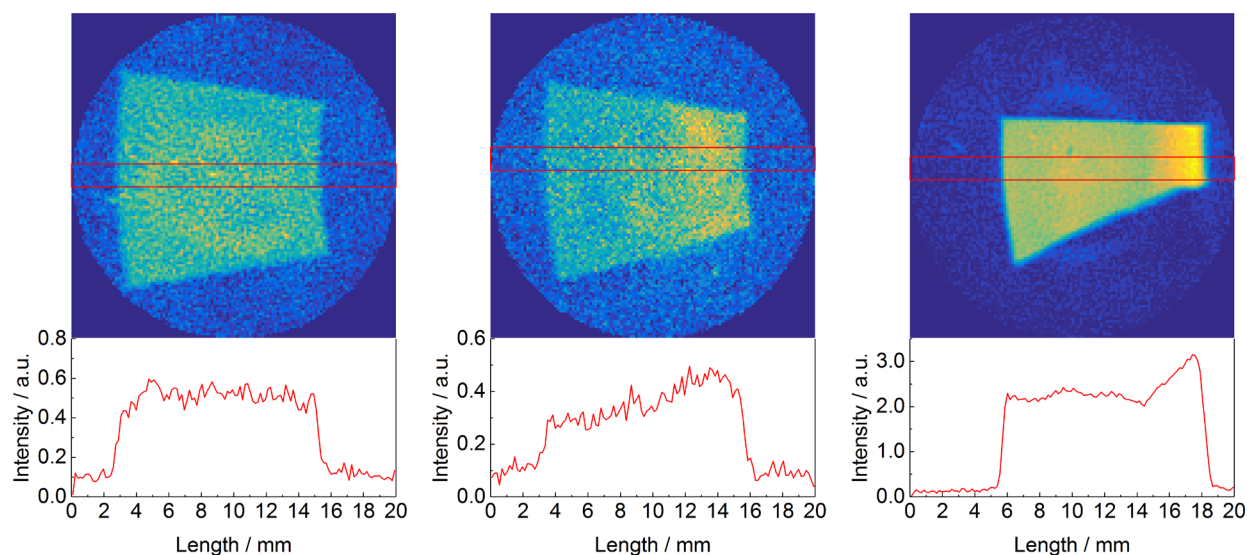


Figure 4. MRI images of samples I (left), II (middle), and III (right). An intensity profile from 10 averaged pixel lines (indicated by the red bars in the 2D images) is shown below each image.

inside the elastomer. The respective profiles confirm this impression. An intensity gradient is visible that is clearly larger than the noise level. A rough estimation of the penetration depth is possible when comparing the signal from the swollen elastomer with the signal from the lubricant-free elastomer. This allows for the determination of the width of the signal gradient, i.e., the penetration depth. The constant (as limited by the SNR) signal, which constitutes the limit of the width of the gradient signal on one side and ideally consists of a signal exclusively from the elastomer, is obtained from the outer sample edge (convex curve) of the respective image. The penetration depth was estimated as 6 ± 1 mm for sample II and 3.6 ± 0.5 mm for sample III. The accuracy of the determination of the penetration depth is clearly proportional to the SNR, which can be improved by more signal averaging and, in consequence, measurement time. No oil penetration was detected in sample I in either the image or in the profile.

The results obtained by MRI are in line with the prior knowledge on the studied material combinations. FKM is one of the most resistant elastomer materials. Hence, with FKM-PAO (sample I), no intrusion of lubricant into the elastomer was detected. The critical FKM-PAG (sample II) combination and the extremely incompatible ACM-PAG (sample III) combination both show a strong signal gradient, which corresponds to permeated lubricant, from the sealing edge toward the inner unloaded areas of the sealing ring.

Figure 5 shows a rendered 3D image of sample IV, which was prepared from the sealing lip of an RSS. It is shown here to demonstrate that samples with complex geometries can also be studied by MRI.

Since the surface of the sample where it was cut from the original RSS is uneven, cf. Figure 5 (left), a suitable imaging region has to be chosen first. Otherwise, the inhomogeneous sample thickness could obscure information on possible oil intrusion. By recording 3D images of the sample, a slab of homogeneous width from the middle of the sample can be selected and investigated for solvent penetration. Such a slab is visualized in Figure 5 on the right. This also works if the sample is slightly curved, as it is the case here, since the measurement directions can be chosen arbitrarily. The resulting 2D projection of the extracted slab is shown in

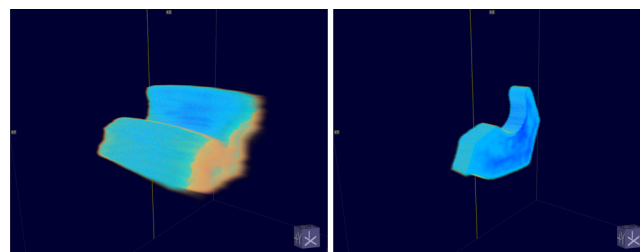


Figure 5. Rendered 3D MRI images of sample IV. (Left) Complete image of the RSS. The fringes on the edges result from the usage of only eight encoding steps in this direction, cf. Table 3. (Right) Selected voxel near the middle of the sample. For the 2D representation, cf. Figure 6.

Figure 6. Again, weak image artifacts are visible around the sample but do not disturb the analysis any further. Two profiles are added for this sample. Here, only one pixel line for each profile is used due to the smaller dimensions of the sample. The vertical profile runs through the sealing lip of the RSS, while the horizontal profile reaches from the oil side into the elastomer, cf. Figure 1. These are the directions from which oil penetration is expected. However, even if intrusion from a different location would occur, it would be detectable in the images. In any case, no oil intrusion was detected in either the profile or the image. The slight intensity variations in the profiles are nonsystematic and are due to limited SNR. This was confirmed by the remaining slabs which could be obtained from the 3D measurement.

Concluding, MRI is a method well-suited for the detection of oil penetration into elastomer seals, even when more complex geometries have to be analyzed. The FKM-PAG (II) and ACM-PAG (III) combinations were identified as incompatible, i.e., showing lubricant intrusion into the seal material.

CONCLUSIONS

The MRI technique and especially the SPI pulse sequence were demonstrated to be capable of producing images of elastomers that had been subjected to a stress test beforehand using a ring cone tribometer. Good image resolution and SNRs

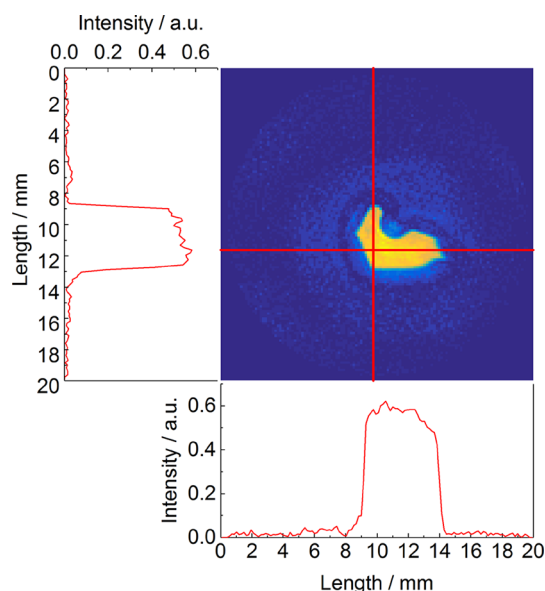


Figure 6. MRI image of sample IV, the 2D depiction of the image shown on the right of Figure 5. Intensity profiles (indicated by the red bars in the 2D image) are shown for two selected pixel lines.

were achieved, and only minor image artifacts were detected. Furthermore, the method can be used to investigate more complex geometries. 3D resolution allows for the identification of suitable acquisition regions to check for lubricant penetration. Incompatible seal–lubricant combinations were identified, and penetration depths of the lubricant into the seal were determined. It is noteworthy that samples I and II were judged correctly to be compatible and incompatible, respectively, based on the results of IRHD measurements (see the Supporting Information). Incompatibility would, however, not have been suspected for sample III. Here, only the MRI results reveal a strong penetration of lubricant into the elastomer, which showcases the capability of the MRI method for the purpose of detecting swelling in elastomers. Compared to the lifetime of a seal in typical gearbox applications,⁸ the tribological tests were of a rather short nature but were nonetheless sufficient to identify quick changes in the elastomer. In future work, additional elastomer–lubricant combinations will be investigated. Staggered screening tests could be used to identify even the diffusion speed or coefficient for a certain elastomer–lubricant combination.

■ ASSOCIATED CONTENT

SI Supporting Information

The Supporting Information is available free of charge at <https://pubs.acs.org/doi/10.1021/acsomega.1c06521>.

Comparison of IRHD hardness in the initial and tribologically stressed state, measured planimetric wear on the elastomer sealing lip, and IRHD hardness in the initial and tribologically stressed states (PDF)

■ AUTHOR INFORMATION

Corresponding Author

Kerstin Münnemann – Laboratory of Engineering Thermodynamics (LTD), TU Kaiserslautern, Kaiserslautern, Rhineland-Palatinate 67663, Germany; orcid.org/0000-0001-5247-8856; Email: kerstin.muennemann@mv.uni-kl.de

0001-5247-8856; Email: kerstin.muennemann@mv.uni-kl.de

Authors

Daniel Bellaire – Laboratory of Engineering Thermodynamics (LTD), TU Kaiserslautern, Kaiserslautern, Rhineland-Palatinate 67663, Germany; orcid.org/0000-0002-0047-6207

Stefan Thielen – Institute of machine elements, gears & transmissions (MEGT), TU Kaiserslautern, Kaiserslautern, Rhineland-Palatinate 67663, Germany

Christoph Burkhart – Institute of machine elements, gears & transmissions (MEGT), TU Kaiserslautern, Kaiserslautern, Rhineland-Palatinate 67663, Germany

Hans Hasse – Laboratory of Engineering Thermodynamics (LTD), TU Kaiserslautern, Kaiserslautern, Rhineland-Palatinate 67663, Germany

Bernd Sauer – Institute of machine elements, gears & transmissions (MEGT), TU Kaiserslautern, Kaiserslautern, Rhineland-Palatinate 67663, Germany

Complete contact information is available at:

<https://pubs.acs.org/10.1021/acsomega.1c06521>

Author Contributions

[▽]These authors contributed equally to this work.

Notes

The authors declare no competing financial interest.

■ ACKNOWLEDGMENTS

Funded by the Deutsche Forschungsgemeinschaft (DFG, German Research Foundation) Project ID 172116086-SFB 926. The authors would like to thank the Forschungsvereinigung Antriebstechnik e.V. (FVA) research association for the support of the project “FVA 578 III: Dynamische Elastomer-Schmierstoffverträglichkeit” (IGF 21650-N), which was funded by the German Federal Ministry of Economics and Energy via the Arbeitsgemeinschaft industrieller Forschungsvereinigungen “Otto von Guericke” e.V. (AiF) within the framework of the program for joint industrial research (IGF). Financial support by the Research Unit NanoKat at the TU Kaiserslautern is gratefully acknowledged.

■ REFERENCES

- (1) Flitney, R. K. *Seals and Sealing Handbook*, 6th ed.; Butterworth-Heinemann: Oxford, U.K., 2014.
- (2) Thielen, S.; Magyar, B.; Sauer, B. Thermoelastohydrodynamic lubrication simulation of radial shaft sealing rings. *J. Tribol.* **2020**, *142*, 052301.
- (3) Siebert, H.; Prem, E. The influence of gear oils on the sealing- and friction behaviour of radial shaft seals. In *17th International Colloquium Tribology: Industrial and Automotive Lubrication*; Technische Akademie Esslingen: Ostfildern, Germany, 2010.
- (4) Mofidi, M.; Kassfeldt, E.; Prakash, B. Tribological behaviour of an elastomer aged in different oils. *Tribol. Int.* **2008**, *41*, 860–866.
- (5) Klaiber, M.; Bauer, M.; Haas, F. Compatibility of oil additives and elastomeric radial lip seals. *Tribol. Schmier.* **2013**, *60*, 60–68.
- (6) Guo, F.; Jia, X.; Huang, L.; Salant, R. F.; Wang, Y. The effect of aging during storage on the performance of a radial lip seal. *Polym. Degrad. Stab.* **2013**, *98*, 2193–2200.
- (7) Guo, F.; Jia, X.; Lv, M.; Wang, L.; Salant, R. F.; Wang, Y. The effect of aging in oil on the performance of a radial lip seal. *Tribol. Int.* **2014**, *78*, 187–194.
- (8) Hermes, J.; Hüttinger, A.; Prem, E. New approval process for dynamic tightness test of gear units: Practical qualifications based on

increased customer requirements & optimized lubricant properties. *Proceedings of the International Conference on Gears 2015* **2015**, 2255, 771–782.

(9) Torbacke, M.; Johansson, A. Seal material and base fluid compatibility: An overview. *J. Synth. Lubr.* **2005**, *22*, 123–142.

(10) Deutsches Institut für Normung e.V.. *Rubber, vulcanized or thermoplastic - Determination of the effect of liquids (ISO 1817:2015)*; DIN ISO 1817:2016-11; Berlin, Germany, 2016; p 31.

(11) International Organization for Standardization. *Rubber - Compatibility between hydraulic fluids and standard elastomeric materials*; ISO 6072:2011; Geneva, Switzerland, 2011; p 19.

(12) Freudenberg Sealing Technologies. *Dynamic oil compatibility tests for Freudenberg radial shaft seals to release the usage in FLENDER-gear units applications (Table T 7300)*; Freudenberg Sealing Technologies: Weinheim, Germany, 2020.

(13) SEW Eurodrive. *Prüfvorschrift 97 118 03 15: Statische und dynamische Prüfungen von Radialwellendichtringen (RWDR)*; SEW Eurodrive GmbH & Co KG: Bruchsal, Germany, 2016.

(14) Hüttinger, A.; Wöpfermann, M.; Hermes, J. Dynamische RWDR Tests neu definiert! In *60th German Tribology Conference 2019: Friction, Lubrication and Wear*, Göttingen, Germany, 2019; Lecture 43.

(15) Smith, G. C.; Park, D.; Titchener, K. J.; Davies, R. E.; West, R. H. Surface studies of oil-seal degradation. *Appl. Surf. Sci.* **1995**, *90*, 357–371.

(16) Burkhart, C.; Weyrich, D.; Thielen, S.; Schollmayer, T.; Sauer, B. Development and optimization of a tribometer for radial shaft seals. *J. Tribol.* **2021**, *143*, 041201.

(17) Burkhart, C.; Schollmayer, T.; van der Vorst, B.; Sansalone, M.; Thielen, S.; Sauer, B. Development of an online-wear-measurement for elastomer materials in a tribologically equivalent system for radial shaft seals. *Wear* **2021**, *476*, 203671.

(18) *NMR Imaging in Chemical Engineering*, 1st ed.; Stapf, S., Han, S., Eds; Wiley, 2005.

(19) Chang, C.; Komoroski, R. A. NMR imaging of elastomeric materials. *Macromolecules* **1989**, *22*, 600–607.

(20) Casanova, F.; Blümich, B. Two-dimensional imaging with a single-sided NMR probe. *J. Magn. Reson.* **2003**, *163*, 38–45.

(21) Adams, A. Analysis of solid technical polymers by compact NMR. *TrAC Trends Anal. Chem.* **2016**, *83*, 107–119.

(22) Blümich, B.; Blümmler, P. NMR imaging of polymer materials. *Makromol. Chem.* **1993**, *194*, 2133–2161.

(23) Blümmler, P.; Blümich, B. NMR imaging of elastomers: A review. *Rubber Chem. Technol.* **1997**, *70*, 468–518.

(24) Knörger, M.; Heuert, U.; Schneider, H.; Bargh, P.; Kuhn, W. Spatially resolved and integral NMR investigation of the aging process of carbon black filled natural rubber. *Polym. Bull.* **1997**, *38*, 101–108.

(25) Klei, B.; Koenig, J. L. NMR imaging of the competitive vulcanization of natural rubber and polybutadiene blends. *Acta Polym.* **1997**, *48*, 199–207.

(26) Shen, Y.; Fei, L.; Zhao, X. Study of γ -irradiation crosslinking of cis-1,4-polybutadiene by NMR microscopy. *Appl. Magn. Reson.* **1995**, *8*, 181–186.

(27) Zhao, J.; Yang, R.; Iervolino, R.; Barbera, S. Changes of chemical structure and mechanical property levels during thermo-oxidative aging of NBR. *Rubber Chem. Technol.* **2013**, *86*, 591–603.

(28) Weisenberger, L. A.; Koenig, J. L. NMR imaging of solvent diffusion in polymers. *Appl. Spectrosc.* **1989**, *43*, 1117–1126.

(29) Clough, R. S.; Koenig, J. L. Observation of polybutadiene rubber structure using NMR imaging. *J. Polym. Sci., Polym. Lett.* **1989**, *27*, 451–454.

(30) Knörger, M.; Arndt, K. F.; Richter, S.; Kuckling, D.; Schneider, H. Investigation of swelling and diffusion in polymers by ^1H NMR imaging: LCP networks and hydrogels. *J. Mol. Struct.* **2000**, *554*, 69–79.

(31) Mansfield, P.; Bowtell, R.; Blackband, S. Ingress of water into solid Nylon 6.6. *J. Magn. Reson.* **1992**, *99*, 507–524.

(32) Webb, A. G.; Hall, L. D. An experimental overview of the use of nuclear magnetic resonance imaging to follow solvent ingress into polymers. *Polymer* **1991**, *32*, 2926–2938.

(33) Valtier, M.; Tekely, P.; Kiéne, L.; Canet, D. Visualization of solvent diffusion in polymers by NMR microscopy with radio-frequency field gradients. *Macromolecules* **1995**, *28*, 4075–4079.

(34) Neutzler, S.; Terekhov, M.; Hoepfel, D.; Oellrich, L. R. NMR investigation of gaseous SF₆ confinement into EPDM rubber. *Magn. Reson. Imaging* **2005**, *23*, 321–323.

(35) Neutzler, S.; Oellrich, L. R. NMR methods investigating the mobility of partly fluorinated hydrocarbons in polymers. *Chem. Eng. Technol.* **2006**, *29*, 840–846.

(36) McDonald, P. J.; Godward, J.; Sackin, R.; Sear, R. P. Surface flux limited diffusion of solvent into polymer. *Macromolecules* **2001**, *34*, 1048–1057.

(37) Gravina, S.; Cory, D. G. Sensitivity and resolution of constant-time imaging. *J. Magn. Reson., Ser. B* **1994**, *104*, 53–61.

(38) Mastikhin, I. V.; Balcom, B. J.; Prado, P. J.; Kennedy, C. B. SPRITE MRI with prepared magnetization and centric-space sampling. *J. Magn. Reson.* **1999**, *136*, 159–168.

(39) Prado, P. J.; Gasper, L.; Fink, G.; Blümich, B. Single-point imaging of vulcanized boundary in rubber. *Appl. Magn. Reson.* **2000**, *18*, 177–185.

(40) Alam, T. M.; Cherry, B. R.; Minard, K. R.; Celina, M. Relaxation nuclear magnetic resonance imaging investigation of heterogeneous aging in a hydroxy-terminated polybutadiene-based elastomer. *Macromolecules* **2005**, *38*, 10694–10701.

(41) Hanfland, J. Simulationswerkzeug zur Abschätzung des Betriebsverhaltens von Radialwellendichtringen. *Forschungsvereinigung Antriebstechnik e.V. (FVA)* **2020**, *574 III*, 19376.

(42) Engelke, T.; Poll, G.; Giese, U. Dichtungsverträglichkeit von Synthetikölen. In *Proceedings of the 15th International Sealing Conference: Innovative Dichtungstechnik - statisch und dynamisch*, Stuttgart, Germany, 2008; pp 109–120.

(43) Engelke, T.; Poll, G. Dichtungsverträglichkeit Synthetiköle - Dichtungsverträglichkeit von Synthetikölen auch unter Berücksichtigung umweltverträglicher Esterschmierstoffe. *Forschungsvereinigung Antriebstechnik e.V. (FVA)* **2006**, *415 I + II*, 14909.

(44) Burkhart, C.; Emrich, S.; Kopnarski, M.; Sauer, B. Excessive shaft wear due to radial shaft seals in lubricated environment. Part I: Analysis and mechanisms. *Wear* **2020**, *460–461*, 203419.

(45) Emid, S.; Creyghton, J. High resolution NMR imaging in solids. *Physica B* **1985**, *128*, 81–83.